AUTOMATED OBJECT DETECTION USING TeLEOS-1 IMAGERIES AND THEIR POTENTIAL APPLICATIONS

CHEW Boon Jin
chew.boonjin@stee.stengg.com
TAN Ren Jie
tan.renjie@stee.stengg.com
ST Electronics (Satcom & Sensor Systems) Pte Ltd,
1 Ang Mo Kio Electronics Park Road, #06-02, Singapore 567710

KEY WORDS: Near-Equatorial Orbit, Image Processing, Imagery Applications, Machine Learning, Computer Vision

ABSTRACT

Since its launch in December 2015 and completion of In-Orbit Test (IOT) in June 2016, TeLEOS-1 has been in operation for over one year. TeLEOS-1, with a 96-minute orbital period at 15 degrees inclination, can deliver high responsiveness coverage to the equatorial belt. TeLEOS-1 is geared for applications such as maritime security and safety, environmental monitoring, humanitarian assistance and disaster relief, and infrastructure development planning and monitoring. Having a high resolution panchromatic camera with a ground sampling distance of 1 by 1 metre, TeLEOS-1 has collected a large imagery database since commencing operations. With a steadily growing database, we can employ image processing techniques to derive higher level information that can be used to provide business intelligence to customers. This paper presents an algorithm which performs automated object detection by utilising feature extraction techniques. Using TeLEOS-1 imagery, the object detection algorithm is applied to perform detection of aeroplanes and oil palms. Using the detection results, additional analysis can be performed to generate comprehensive reports, such as estimating oil palm health and yield rate or global oil storage, for decision making.

1 INTRODUCTION

AgilSpace is the signature brand for satellite and remote sensing products and services offered by ST Electronics (Satcom & Sensor Systems) Pte Ltd [AgilSpace, 2014]. We offer design, manufacturing and integration of satellites and satellite subsystems, ground control centre operations, launch management services and value-added geospatial service and data analytics.. We also offer a wide range of imagery products from our very own TeLEOS-1 and our various partners' satellites. Till date, our partners' satellites include Spot 6, Spot 7, Pleiades 1A & 1B, RadarSat2, Cosmo Skymed, TerraSAR-X, and KompSat 2, 3, 3A and 5.

Firstly, the paper describes the methodology used to perform object detection in the Section 2. In Section 3, we show the detection results of aeroplanes and oil palms from satellite images. Lastly, we conclude with discussions on potential applications of this object detection in Section 4. However, before delving into the detailed discussion, we would like to formally introduce the source of our imagery, TeLEOS-1, and our in-house developed online platform, AgilSpace GeoPortal.

TeLEOS-1 is a commercial earth observation satellite carrying an Electro-Optical (EO) sensor flying at Low Earth Orbit (LEO) at an inclination of 15 degrees. With a quick mean revisit time of 12 - 16 hours, TeLEOS-1 offers high responsiveness to the equatorial belt. At nadir, the panchromatic EO sensor has a swath of 12 km and offers a ground sampling distance of 1 metre. TeLEOS-1 offers three imaging modes: multi-point, strip and area imaging. [Seah et al., 2016]

AgilSpace GeoPortal, a one-stop e-commerce platform for all imagery needs, was launched on 31 May 2016 at CommunicAsia 2016. AgilSpace GeoPortal allows users to view and purchase archived imagery or request for new tasking over their area of interest. Payment options can be by credit card, cheque, telegraphic transfer or purchase orders. The AgilSpace Geoportal can be accessed directly at https://www.agilspace.com:8080/.

2 OBJECT DETECTION

2.1 Introduction

With daily imagery acquisition, the imagery archive is growing steadily. Such imagery are geolocation and time tagged and they offer exciting opportunities to perform different analyses such as change detection, environmental monitoring, land use classification, hot-spot detection and monitoring, etc.. Insights from such analyses create the basis for developing customised solutions for interested parties. Another information which can be extracted from satellite imagery is a collation of Object of Interest (OOI). Some examples of OOI visible from space are aeroplanes, ships, buildings, oil storage tanks, oil palms, etc.. By extracting these OOI, we can utilise more advanced image processing and machine learning techniques to generate meaningful statistics such as monitoring levels in oil storage tanks or agricultural health and stocks.

2.2 Methodology

The methodology employed in this paper is inspired by the object detection framework proposed by Paul Viola and Michael Jones [Viola and Jones, 2004]. The high accuracy and computation speed they achieved for facial recognition showed great promises in the general object detection problem. The detection of OOI such as aeroplanes and ships have similar challenges to face detection as they have a generic shape with small variations in sizes and spectral return. The methodology can be summarized into three modules: collection of training data; training process and performance verification. In the following sections, we shall look at these modules in greater detail.

2.3 Generation of Training Data

Though there are many datasets of different classes on the Internet, these images are usually acquired from ground view and hence not suited for the top view of satellite imagery. The training and test datasets are independent subsets of a general dataset comprising of positive and negative images. Positive images are images containing a single instance of the OOI, while negative images can contain anything with the exception of the OOI. Generation of positive and negative images are steered by the requirements of the selected OOI. A common guideline in generating the set of positive images is to ensure that it should sufficiently cover most variations of the object such as shape, size and colour. This would ensue a high true positive rate. In generating the set of negative images, we should focus on objects which have similar statistical properties and spatial intensity distribution as the OOI. Objects which appear in close proximity to the OOI should be added into the set of negative images as well. This would allow the trained classifier to be capable of performing detection at a high accuracy. In Figure 1, we can see some examples of negative images chosen for the training of an aeroplane detector. The training and testing datasets are resized to a fixed size before beginning the training process as the feature encoding process (as described in Section 2.4 below) operates on a single window size.

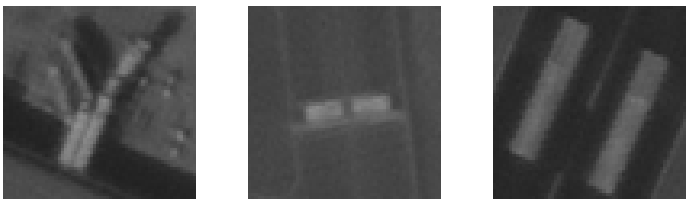

(a) (b) (c)

Figure 1: Examples of Negative Images for Training of an Aeroplane Detector

2.4 Object Detection Algorithm

There are many different object detection frameworks developed in the past few decades and in recent years, there have been much interest in deep learning. In this paper, the object detection algorithm implemented in the Open Source Computer Vision (OpenCV) Library was used to perform both the training and detection [OpenCV, 2011].

During the detection process, a trained classifier produced by the algorithm would decide if an input image contains the OOI. This trained classifier consists of several stages arranged in a cascaded structure. The results of each

stage consists of a boosted set of binary decision trees with at least one level. Boosting refers to a weighted voting of this set. The boosting process would result in a strong yet simple classifier. The overall training process can be summarised as follows:

1. an initial batch of training images are chosen to train the current stage, and this stage would be appended to the cascade structure
2. training images detected as positive by the current cascade structure would be passed as training images for the next stage
3. the process is repeated till a specified threshold is met where the algorithm would break

By training as such, the detection process would get more stringent as it goes down the stages as each stages gets better at distinguishing the OOI. In other words, a test candidate would be subjected to higher bar as it goes through the cascade structure.

The inputs to the binary decision trees are values of the training images extracted by a set of Haar-like features. These Haar features differs from each other by shape (as shown in Figure 2), size (via scaling), and position within the image window. These values are calculated by taking the difference of the sums of pixel intensities in the white and black rectangles. The algorithm uses integral images - an alternate image representation - allowing for rapid calculation of the sum of pixel intensities within the rectangular region.

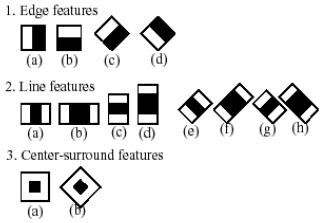

Figure 2: Examples of Haar Features. Retrieved from url (http://docs.opencv.org/2.4/modules/objdetect/doc/cascade_classification.html) on 26-Aug-2017

The cascade structure can be visualized as a series of multiple sieves with decreasing sieve sizes. The early stages would quickly reject majority of the negative test images that has a low probability of being true positive. This would leave behind a smaller test set consisting of complex negative images which are harder to differentiate from positive images. These later stages are trained specifically, as discussed above, to make these more difficult decisions. By having such a cascade structure, rapid detection can be achieved with high accuracy.

After completion of the training, the trained classifier is used to perform detection on a test dataset or a satellite image to verify its performance. The results from detection of the test dataset, as described in detail in the following section, provide statistics on the trained classifier. The detection on the satellite image provides a visual insight into the detection performance. As the satellite image is much larger than the size of training images, a set of test images is extracted before passing through the trained classifier. This set of test images is generated by sliding a small window (of same size as the training dataset) across the satellite image.

2.5 Performance Verification

The performance of the trained classifier can be measured from the detection results of the test dataset. Four values can be determined directly from the detection results: True Positive (TP) represent the number of positive images detected; True Negative (TN) represent the number of negative images not detected; False Negative (FN) represent the number of positive images not detected and False Positive (FP) represent the number of negative images detected. These four values constitute the confusion matrix. Other performance metrics such as precision, recall (or True Positive Rate (TPR)), False Positive Rate (FPR), and accuracy can be determined from the confusion matrix as described by Equations 1 to 4 below.

$$\text{Precision} = \frac{\text{TP}}{\text{TP} + \text{FP}} \tag{1}$$

$$\text{Recall (TPR)} = \frac{\text{TP}}{\text{TP} + \text{FN}} \tag{2}$$

$$\text{FPR} = \frac{\text{FP}}{\text{FP} + \text{TN}} \tag{3}$$

$$\text{Accuracy} = \frac{\text{TP} + \text{TN}}{\text{TP} + \text{FN} + \text{TN} + \text{FP}} \tag{4}$$

3 RESULTS AND DISCUSSION

3.1 Overview

The object detection methodology described above was applied for two different OOIs - aeroplanes and oil palms. These two OOIs are chosen as they can be distinctly recognised from satellite images and they have limited variations. The estimated pixel size of aeroplanes and oil palms can be determined from their actual size. Oil palms with an age of 15 years have an estimated average crown diameter of 10.3 metres [Korom et al., 2016] whereas Aeroplanes have slightly larger range of sizes from about 10 metres in length and wingspan (light aircraft) to over 50 metres in length and wingspan (large commercial aeroplanes such as Boeing 777-300ER has a length of 73.9 metres and wingspan of 64.8 metres [Boeing, 2015]). With TeLEOS-1 sensor resolution of 1 metre by 1 metre, oil palms will appear about 10 by 10 pixels, while planes can range from 10 by 10 pixels to beyond 50 by 50 pixels.

3.2 Aeroplane Detection

TeLEOS-1 images covering major airports across the equatorial belt were retrieved from the image database, and the dataset of positive and negative images were generated. From this dataset, 600 each of positive and negative images were moved to the test dataset while the remaining images were pushed for training. The training dataset comprises of 3000 positive images and 10000 negative images. The test dataset was then tested using the trained classifier and the results are recorded. Table 1 shows the confusion matrix generated from the test results. The performance metrics (as defined in Section 2.5) were determined as shown in Table 2. A TeLEOS-1 image over El Dorado International Airport in Bogota, Colombia was tested to demonstrate visual confirmation of the trained classifier's performance. Figure 3 shows the detection results on an area within the airport.

Table 1: Confusion Matrix for Aeroplane Detection

		Predicted	
		No	Yes
Actual	No	TN = 590	FP = 10
	Yes	FN = 70	TP = 530

Table 2: Performance Metrics for Aeroplane Detection

Precision	98.1%
Recall	88.3%
FPR	1.7%
Accuracy	93.3%

A low FPR of 1.7% shows that our classifier is very good at distinguishing negative images, even those that have similar statistical properties as our OOI. This is mainly credited to cascade structure formed during the training stages. A value of 88.3% for recall demonstrates satisfactory performance in detection of aeroplanes with some challenges remain to be overcome. Challenges like orientation of plane, physical dimensions, positions and shapes of the wings could potentially be aggravating factors reducing the performance of the trained classifier.

3.3 Palm Trees

A TeLEOS-1 image over an oil palm plantation in Pahang, Malaysia was retrieved from the image database for the generation of the training dataset. A total of 17000 positive and 100000 negative images were generated. The training and testing were conducted and the confusion matrix was generated. Figure 4 shows the performance of the trained

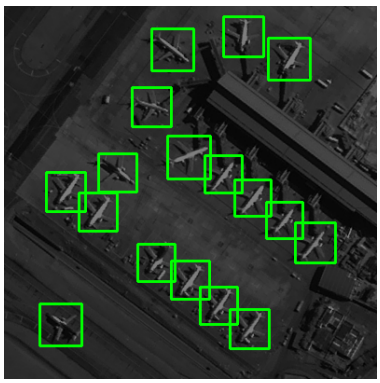

Figure 3: Results of Aeroplane Detection

classifier on an area within TeLEOS-1 image over Pahang in Malaysia. A test dataset, comprising 1000 each of positive and negative images, was generated from the image over Pahang. The detection was performed and the confusion matrix and performance metrics are shown in Tables 3 and 4.

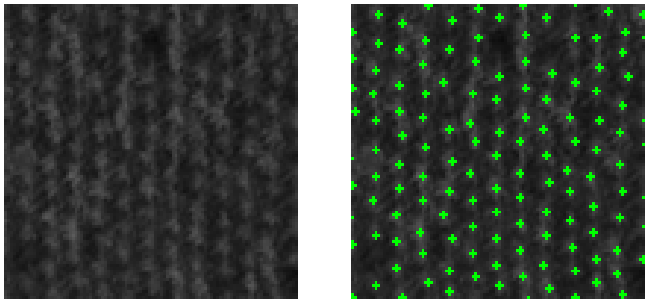

(a) (b)

Figure 4: Results of Oil Palm Detection

Table 3: Confusion Matrix for Oil Palm Detection in Malaysia

		Predicted	
		No	Yes
Actual	No	TN = 972	FP = 28
	Yes	FN = 3	TP = 997

Table 4: Performance Metrics for Oil Palm Detection in Malaysia

Precision	97.2%
Recall	99.7%
FPR	2.8%
Accuracy	98.4%

High performance in both detection of oil palm and rejection of negative images were obtained. To prove the consistency of the performance of the trained classifier, another TeLEOS-1 image over Bengkulu, Indonesia, was retrieved and the test dataset comprising 1000 each of positive and negative images was generated. The confusion matrix and performance metrics for this test dataset are shown in Tables 5 and 6.

A sharp drop in recall to 69.7% was observed while the FPR, at 3.2%, was close to the test dataset generated from the image over Malaysia. The drop in recall could likely be due to the different location imaged, sun position, and the satellite position at the instance of imaging. The relevant imaging and sun parameters at the instance of imaging was

Table 5: Confusion Matrix for Oil Palm Detection in Indonesia

		Predicted	
		No	Yes
Actual	No	TN = 968	FP = 32
	Yes	FN = 303	TP = 697

Table 6: Performance Metrics for Oil Palm Detection in Indonesia

Precision	95.6%
Recall	69.7%
FPR	3.2%
Accuracy	83.2%

Table 7: Imaging Parameters for TeLEOS-1 image over Malaysia and Indonesia

Location	Sun Elevation	Sun Azimuth	Satellite Elevation	Satellite Azimuth
Pahang, Malaysia	54.27 deg	284.20 deg	57.05 deg	36.76 deg
Bengkulu, Indonesia	58.88 deg	33.24 deg	75.19 deg	234.76 deg

retrieved from the imagery meta-data and are shown in Table 7.

Imaging at different locations could mean the oil palm are of different species and of a different age, leading to a different view of oil palms from space. Also, the spacing between oil palms may be different, further complicating the detection process. A different sun position at imaging time would alter the illumination source point, while a different satellite position would shift the view point. A combination of the variation arising from these two positions would result in substantial variation in the appearance of oil palms within the image. Such variation are not possible to be captured in a single image, which would possibly explain the sharp drop in recall upon testing on other images.

3.4 Discussion

Satellite images, though capable of providing a wide coverage with a single image, have their own inherent challenges. Presence of cloud makes imaging of surface difficult for EO sensors. Regions covered by clouds' shadow results in very low contrast. As TeLEOS-1 operates in the equatorial belt, ground targets have multiple imaging opportunities across the day. Hence different imaging time would result in different ground illumination, causing variations to shadow position and length.

Besides the problems resulting from usage of different satellite images, the selected OOI has its own challenges as well. If planted too closely, crowns of neighbouring oil palms would merge and individual oil palm may be indistinguishable. Also, occlusion of the OOI would pose a huge difficulty in detection. In addition, varying imaging angles would provide a different view point which complicates the detection process.

Although good performance has been observed currently, it can be further improved by performing additional preprocessing. Image segmentation can be performed initially to extract either airports or oil palm plantations, following that the object detection process can be applied on these selected areas to detect the respective OOI.

4 APPLICATIONS

Extensive land coverage by satellite images bring about much potential applications in many fields such as land use classification, humanitarian aid and disaster rescue, environmental monitoring, agricultural applications, change detection and tracking, etc. Object detection in satellite images provides an alternate direction to some of these applications. Results from aeroplane detection can directly be used to perform counting of aeroplanes in the airport, or even performing identification of the plane models within the airport. Such identification process allows listing of common plane models within the airport and they can be used to gauge the passenger flow in the airport or even determine the population crowd in the nearby cities. Identification of the plane models also provide insights into the use of the airports, whether it is for military, commercial or private.

Oil palms, upon detection, can be geotagged. Additionally, using multi-spectral imagery over the same area, we

can perform Normalised Difference Vegetation Index (NDVI) on individual trees providing a record of each oil palms health. Problems such as infestation or infection of the oil palms can be detected and resolved early. Also, using the detection results of each oil palm, detailed studies can be done on the correlation between the crown sizes and ages. Such information would provide plantation owners with more insights on their plantations, allowing them to make profit enhancing decisions such as space maximisation for cash crops, resource management, focusing more on areas requiring attention, etc. Such information will also provide the plantation investors insights into their assets and their yields. Market analysts can also use this information to predict the production output and hence anticipate the market price. [GDA Corp, 2016]

Estimation of the oil levels within oil tanks can be done by measuring the shadow the rim cast on the floating roof and the shadow cast on the ground [SkyWatch, 2016]. With the diameter (obtained directly from the image as the image resolution is known) and the solar elevation, the oil levels and hence volume can be determined. Such analytics are not possible if the oil tanks are not detected in the first place. Here, the object detection algorithm locates each oil tank automatically, allowing the oil level analysis to be performed. The oil storage across the globe can be determined and such information would better equip investors in oil prices anticipation. [Orbital Insights, 2016]

5 CONCLUSION

All in all, the object detection algorithm discussed in this paper has shown promising results in its ability to detect aeroplanes and oil palms from TeLEOS-1 images. With an increasing archive of imagery, this algorithm offers one form of data extraction for more advanced data analytics and machine learning. The results of object detection would greatly aid us by providing the basis to derive high order information and deliver high value services.

With such encouraging results obtained, more advanced machine learning techniques such as deep neural networks can be used for more complex classification processes. The object detection algorithm allows easy extraction of objects from different classes, which would generate large datasets for training deep networks. With the object detection algorithm as a first step, having these deep networks are potentially the next step forward in generating more value-added geospatial products.

References

[AgilSpace, 2014] AgilSpace (2014). AgilSpace Website. www.agilspace.com. (Date last accessed 26-August-2017).

[Boeing, 2015] Boeing (2015). 777-200LR/-300ER/-Freighter Airplane Characteristics for Airport Planning.

[GDA Corp, 2016] GDA Corp (2016). Agricultural Business Intelligence. http://www.gdacorp.com/agricultural-intelligence. (Date last accessed 26-August-2017).

[Korom et al., 2016] Korom, A., Phua, M.-H., and Matsuura, T. (2016). Relationships between Crown Size and Aboveground Biomass of Oil Palms: An Evaluation of Allometric Models. *Sains Malaysiana*, 45(4):523–533.

[OpenCV, 2011] OpenCV (2011). Haar Feature-based Cascade Classifier for Object Detection. http://docs.opencv.org/2.4/modules/objdetect/doc/cascade_classification.html. (Date last accessed 26-August-2017).

[Orbital Insights, 2016] Orbital Insights (2016). World Oil Storage Index. https://orbitalinsight.com/solutions/world-oil-storage-index/. (Date last accessed 26-August-2017).

[Seah et al., 2016] Seah, P. H., Tan, W. C. J., Chang, J. R., and Tan, T. C. M. (2016). TeLEOS-1: First Commercial Earth Observation Satellite in Near Equatorial Orbit. *37th Asian Conference on Remote Sensing, Colombo, Sri Lanka*.

[SkyWatch, 2016] SkyWatch (2016). 4 Ways Satellite Imagery Is Changing How We Invest. https://www.skywatch.co/blog/2016/7/24/4-ways-satellite-imagery-is-changing-how-we-invest. (Date last accessed 26-August-2017).

[Viola and Jones, 2004] Viola, P. and Jones, M. (2004). Robust Real-time Object Detection. *International Journal of Computer Vision*, 57(2):137–154.